

Phonon engineering in graphene and van der Waals materials

Alexander A. Balandin

The following article is based on the MRS Medal Award presentation given by Alexander A. Balandin on December 4, 2013, at the Materials Research Society Fall Meeting in Boston. Balandin was recognized for his "discovery of the extraordinary high intrinsic thermal conductivity of graphene, development of an original optothermal measurement technique for investigation of thermal properties of graphene, and theoretical explanation of the unique features of the phonon transport in graphene."

Phonons—quanta of crystal lattice vibrations—reveal themselves in electrical, thermal, optical, and mechanical phenomena in materials. Phonons carry heat, scatter electrons, and affect light–matter interactions. Nanostructures opened opportunities for tuning the phonon spectrum and related properties of materials for specific applications, thus realizing what was termed phonon engineering. Recent progress in graphene and two-dimensional van der Waals materials has led to a better understanding of phonon physics and created additional opportunities for controlling phonon interactions and phonon transport at room temperature. This article reviews the basics of phonon confinement effects in nanostructures, describes phonon thermal transport in graphene, discusses phonon properties of van der Waals materials, and outlines practical applications of low-dimensional materials that rely on phonon properties.

Phonons and phonon engineering in nanostructures

Phonons, which are quanta of crystal lattice vibrations, affect the thermal, electrical, optical, and mechanical properties of solids.[1] In semiconductors, acoustic and optical phonons limit electron mobility and influence their optical response. Acoustic phonons are the main heat carriers in electrical insulators and semiconductors. Long-wavelength acoustic phonons constitute the sound waves. Similar to electrons, phonons are characterized by their dispersion relation $\omega(\mathbf{q})$, where ω is angular frequency, and $\mathbf{q}$ is a wave vector of a phonon. In bulk semiconductors with α atoms per unit cell, there are 3α phonon dispersion branches for each value of $\mathbf{q}$. Three types of vibrations describe the motion of the unit cell and form three acoustic phonon branches. The other $3(\alpha-1)$ modes describe the relative motion of atoms inside the unit cell forming the optical phonon branches. Examples of the phonon dispersion branches are shown in **Figure 1**.

Acoustic polarization branches are commonly referred to as longitudinal acoustic (LA) and transverse acoustic (TA) phonons. One can also distinguish between longitudinal optical (LO) and transverse optical (TO) phonons. In the case of two-dimensional (2D) material systems such as graphene, the out-of-plane transverse vibrations are denoted as *z*-axis acoustic (ZA) phonons. In the long-wavelength limit, acoustic phonons in bulk crystals have nearly linear dispersion, which can be written, in the Debye approximation, as $\omega = V_S q$, where V_S is the sound velocity, while the optical phonons are nearly dispersionless and have a small group velocity $V_G = d\omega/dq$. Acoustic phonons usually carry most of the heat in semiconductors.[2]

Spatial confinement of acoustic phonons in nanostructures affects their energy dispersion[3–6] and modifies acoustic phonon properties such as phonon group velocity, polarization, and density of states (DOS). As a result, spatial confinement changes the way acoustic phonons interact with other phonons, defects, and electrons.[3–6] This creates opportunities for engineering the phonon spectrum in semiconductor nanostructures for improving their electrical, thermal, or mechanical properties. In order to understand when the structure size starts to affect phonon properties and phonon transport, one can recall that the average phonon mean free path (MFP) in semiconductors is ~50–300 nm near room temperature (RT). At this length scale, the acoustic phonon transport is affected

Alexander A. Balandin, University of California–Riverside, USA; balandin@ee.ucr.edu
DOI: 10.1557/mrs.2014.169

© 2014 Materials Research Society

https://doi.org/10.1557/mrs.2014.169 Published online by Cambridge University Press

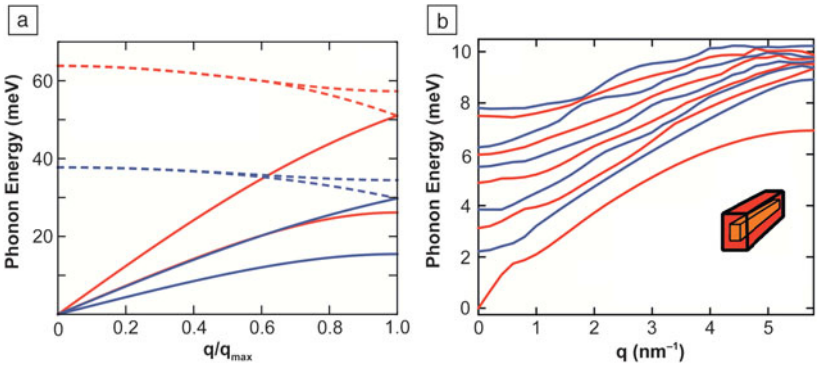


Figure 1. Illustration of phonon confinement effects. (a) Phonon energy dispersion in bulk silicon (red curves) and germanium (blue curves) crystals along the (110)-crystallographic direction, calculated using the five-parameter Born-von Karman model. Acoustic phonon branches are shown with the solid lines, while optical phonon branches are shown with dashed lines. (b) Dispersion of confined phonons in silicon nanowires coated with germanium. The cross-sections of the nanowire core and outside shell are 3.26 nm × 3.26 nm and 4.88 nm × 4.88 nm, respectively. Note that by changing the lateral dimensions of the nanowire and barrier shell, the shape of the cross-section, and the acoustic impedance mismatch at the interface, one can tune the phonon dispersion and group velocity.

by phonon scattering from the boundaries of the material sample. The phonon–boundary scattering rate can be evaluated as $1/\tau_B = (V_S/D)[(1-p)/(1+p)]$, where D is the nanostructure size and $0 \le p \le 1$ is the specularity parameter defined as a probability of specular and diffuse scattering at the boundary.[1,2] In nanostructures, where the phonon–boundary scattering is dominant, thermal conductivity scales with the size (D) as $K_p \sim C_p V_S \Lambda \sim C_p V_S^2 \tau_B \sim C_p V_S D$, where C_p is the thermal heat capacity at constant pressure, and Λ is the phonon MFP.

Another important scaling parameter for phonons is the typical wavelength of the thermal phonon $\lambda_T = 1.48\,\hbar V_S/(k_B T)$, which is ~1–2 nm ($\hbar$ is Planck's constant, k_B is the Boltzmann constant, and T is absolute temperature).[7] Phonon transport becomes more interesting when the structure dimensions are reduced to the scale of λ_T. The spatial confinement of acoustic phonons and mode quantization open an opportunity for increasing or decreasing the thermal conductivity and electron mobility via engineering the phonon spectrum.[8–22] The electron mobility, limited by the phonons in silicon nanowires[23] or thin films,[24] can be enhanced via suppression of electron–phonon interactions in nanostructures with acoustically hard barriers.[23,24] Similarly, one can increase or decrease the heat conduction properties of nanowires or thin films by using acoustically mismatched barrier layers.[25,26] The predictions for thermal and electronic conduction in semiconductor nanostructures in the phonon confinement regime, initially made within the elastic continuum approximation,[3–6,8–11,21–31] have been confirmed by independent molecular-dynamics simulations[32] and direct experimental measurements on Ge-Si core–shell nanowires.[33]

Figure 1 presents an example of the modification of the bulk phonon dispersion in semiconductors when one utilizes a nanowire with acoustically mismatched barriers.[5,6,8–11] The acoustic impedance is defined as $\zeta = \rho V_s$, where ρ is the mass density. Engineering of the optical phonons in nanostructures via the boundary conditions requires different approaches than engineering of the acoustic phonons. In the long-wave limit, the optical phonons correspond to the motion of atoms within the same unit cell, which cannot be changed by imposing new outside boundaries. However, the electron–phonon scattering rates can be modified by tuning the energy difference between the confined electron energy levels with respect to the optical phonon energy.[12] This effect—referred to as a "phonon bottleneck"—can be used for optimization of solid-state lasers or other devices. Heterostructures, which consist of layers with distinctively different optical phonon energies, allow one to localize optical phonons within their respective layers, which can also be used for practical purposes.[5] The advent of graphene and other two-dimensional (2D) materials (also referred to as van der Waals materials, as the atomic planes are bound by weak van der Waals forces), has significantly increased the opportunities for controlling the phonon spectrum, including the higher energy optical phonon branches. This article gives a few examples of phonon transport and phonon engineering in graphene and 2D van der Waals materials.

Phonons and thermal transport in graphene

The first measurements of the thermal conductivity of graphene revealed unusually high values of thermal conductivity in the range from 2000 W mK^{-1}–5000 W mK^{-1} near RT.[34,35] The values measured for high-quality, large suspended graphene samples (lengths above 10 μm) exceeded those for basal planes of graphite.[34–36] The thermal transport was dominated by acoustic phonons owing to the exceptionally strong sp^2 covalent bonding of graphene's lattice. There might be an inherent ambiguity in the absolute values of the thermal conductivity of graphene due to the uncertainty in the definition of the thickness of one atomic plane. However, the differences in the physics of phonon propagation in bulk and 2D materials resulting in unusual features of phonon heat conduction in graphene are real. The experimental observation of large thermal conductivity was explained theoretically by the specifics of the low-energy (long wavelength) phonon transport.[37–39] Low-energy acoustic phonons in graphene, which substantially contribute to heat conduction, have exceptionally large MFP.[37–41] The phonon–phonon scattering due to crystal lattice inharmonicity, referred to as Umklapp scattering, is very weak for such phonons in 2D graphene.[42–44] Numerous molecular dynamics (MD) simulations confirmed the conclusion that the intrinsic thermal conductivity of atomic

https://doi.org/10.1557/mrs.2014.169 Published online by Cambridge University Press

planes of sp^2 bound atoms decreases when one switches on the interaction between the planes.[44,45]

Experimental studies of the thermal properties of graphene were made possible with the development of the optothermal technique based on Raman spectroscopy (see **Figure 2**). In this technique, a Raman spectrometer acts as a thermometer measuring the local temperature rise in graphene in response to the laser heating.[34,35] In the original experiments, the laser power absorbed in graphene was determined from the ratio of the integrated Raman intensities of the G peak for graphene and reference graphite.[34,35] Independent measurements conducted by other research groups used modified optothermal techniques where the absorbed power was measured by a detector placed under the suspended portion of graphene.[46,47] The thermal conductivity values of the suspended graphene reported by different groups were consistently high.[35,42,46,48] The discrepancy was attributed to differences in the sample size, quality, and strain distribution.[35] The thermal conductivity of graphene supported on a Si/SiO_2 substrate was lower ($K \approx 600$ W mK^{-1} at RT) than in suspended graphene owing to substrate scattering effects.[49]

A promising approach for phonon engineering in low-dimensional materials is changing the isotope composition. Naturally occurring carbon materials are made up of two stable isotopes, ^{12}C (~99%) and ^{13}C (~1%). Isotopically modified graphene containing various percentages of ^{13}C were synthesized by a chemical vapor deposition technique.[50–52] The frequency ω of the optical phonon at the Brillouin-zone (BZ) center varies with the atomic mass, M, as $M^{-1/2}$, making the Raman shift for ^{13}C graphene approximately 64 cm^{-1} smaller than that for ^{12}C.[48] This explains why Raman spectroscopy is a powerful tool for monitoring the isotope composition of isotopically modified carbon allotropes. The thermal conductivity of isotopically pure ^{12}C (0.01% ^{13}C) graphene, measured by the optothermal technique,[35] was higher than ~4000 W mK^{-1} near RT, and more than a factor of two higher than the thermal conductivity of graphene sheets composed of a 50%-50% mixture of ^{12}C and ^{13}C.[48] The evolution of the thermal conductivity with the isotope content was attributed to the changes in the phonon–point defect scattering rate via the mass-difference mechanism. The change in isotope composition affects phonons but does not influence electrons. For this reason, controlling the isotope composition allows one to tune phonon propagation without affecting electron transport. Engineering of the phonon spectrum in graphene by varying isotope composition can improve prospects for applications of graphene for thermal management and thermoelectric energy conversion.

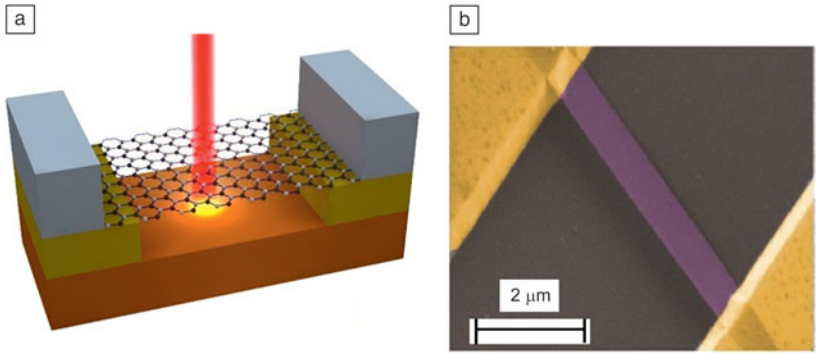


Figure 2. Optothermal technique for measuring thermal conductivity of graphene and thin films. (a) Schematic of the experimental setup for optothermal measurements where the excitation laser light is focused on graphene suspended across a trench in a silicon wafer. The laser power absorbed in graphene induces a local hot spot and generates a heat wave propagating toward the graphite or metal heatsinks. (b) Scanning electron microscope image of a graphene flake suspended over a trench. Pseudo-colors are used for clarity: Violet corresponds to graphene, yellow to silicon oxide, and black to the silicon substrate.[35]

Phonons in van der Waals materials

The successful exfoliation of graphene[53,54] and discoveries of its unique electrical and thermal properties have motivated searches for other quasi-2D materials with interesting characteristics.[55–59] As a group, layered van der Waals materials[55] can be cleaved mechanically or exfoliated chemically by breaking the relatively weak van der Waals bonding between the layers. The resulting thin films can be re-stacked into superlattice-type structures with various properties. Exfoliated quintuples—five atomic layers—of bismuth telluride (Bi_2Te_3) revealed thermoelectric and topological insulator phenomena substantially different from those of bulk Bi_2Te_3 crystals.[56,60–62] The changes are substantial not only for electronic states but for phonons as well. Modification of the acoustic phonon spectrum in the atomically thin films affects their heat conduction properties, while the changes in the optical spectrum can be used for nano-metrology purposes.

Figure 3 shows an example of the use of Raman spectroscopy for assessing the quality and thickness of exfoliated few-quintuples layers (FQLs) of Bi_2Te_3.[61] For investigation of the topological insulator properties, it is beneficial to have FQL thin films. An additional peak appears at ~117 cm^{-1} in FQLs and its intensity, normalized to the intensity of E_g^2 (the most pronounced feature in the spectrum), grows with decreasing FQL thickness. This A_{1u} peak is composed of TO phonons at the BZ boundary (Z point). The A_{1u} peak is IR active but not Raman active in bulk Bi_2Te_3.[63,64] It appears in FQL materials owing to crystal symmetry breaking. Since a single quintuple is inversely symmetric, the crystal symmetry breaking is likely related to the loss of infinite crystal periodicity due to interfaces and corresponding relaxation of the phonon wave vector $q = 0$ selection rule. The E_g^2 (TO) peak is composed of regular BZ-center phonons originating in the "bulk" of the film. As a result, the ratio of the peak intensities, $I(A_{1u})/I(E_g^2)$, increases with decreasing thickness (H) because of the decreasing interaction volume $V = S \times H$

https://doi.org/10.1557/mrs.2014.169 Published online by Cambridge University Press

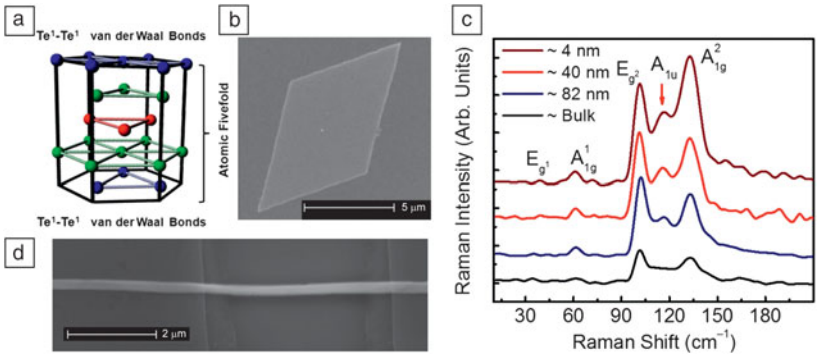


Figure 3. Raman spectroscopy as a nano-metrology tool for atomically thin films of van der Waals materials. (a) Crystal structure of an individual quintuple of Bi_2Te_3. Bismuth atoms are shown in green color, while telluride atoms are indicated in red and blue. The bonding to the next quintuple is via the outside (blue) telluride atoms. (b) "Graphene-like" exfoliated few-quintuple layer of Bi_2Te_3 on a silicon substrate. (c) Evolution of the Raman spectrum of a Bi_2Te_3 thin film as its thickness decreases to the few-quintuple scale. (d) A Bi_2Te_3 thin-film ribbon suspended across a trench in a silicon wafer.[56,60–62]

(where S is the cross-sectional area of the laser spot), which defines $I(E_g^2)$ for H smaller than the light penetration depth in a given material. This dependence makes possible non-destructive, rapid, and reliable nano-metrology of FQL materials after calibration with atomic force microscopy (AFM).[61]

The graphene-like exfoliation of thin films from Bi_2Te_3 crystals followed by re-assembly into "pseudo-superlattices" of the stacks of such van der Waals films resulted in an improved thermoelectric figure of merit.[62] The in-plane thermal conductivity of the stacks decreased by a factor of ~2.4 at RT as compared to the bulk, or by ~3.5 for the cross-plane value. It was concluded that the reduction of the phonon thermal conductivity without degradation of the electrical transport properties was responsible for the observed improvement of the thermoelectric efficiency. The film thinning to FQL and tuning of the Fermi level can potentially lead to achieving high thermoelectric efficiency.

Phonons and thermal transport in MX_2 thin films

An interesting subgroup of inorganic van der Waals materials is the layered transition metal dichalcogenides MX_2, where M = Mo, W, Nb, Ta, or Ti and X = S, Se, or Te.[65] Some of these materials, with strong coupling between electron and phonon states, reveal charge density wave (CDW) effects in the temperature range from ~100 K to RT.[66] CDW is a symmetry-reducing ground state most commonly found in layered materials. It was recently found that decreasing the thickness of titanium diselenide ($TiSe_2$) thin films allows one to significantly increase the transition temperature (T_P) to the CDW phase.[67] This advance opens the possibility of CDW-based devices that can operate near or at RT. The changes in the phonon spectra in this group of 2D materials can also be used for nanometrology purposes. They should also be taken into account while assessing the thermal properties of these films and considering their possible device applications.

Figure 4a shows Raman spectra of $TaSe_2$ for nine exfoliated thin films with different thicknesses H, ranging from a few nm to >250 nm.[68] The thicknesses of the exfoliated films were measured by AFM. The 2H-$TaSe_2$ crystal possesses 12 zone center lattice vibrational modes. Four of these modes (E_{2g}^2, E_{1g}, E_{2g}^1, and A_{1g}) are Raman active. A pronounced Si peak from the substrate also appears at 522 cm^{-1}. The intensity of the BZ-center Si peak is proportional to the interaction volume. The ratio of the intensity of the Si peak to that of A_{1g} or E_{2g} can be used for determining the thickness of the exfoliated film. Figure 4b presents the ratio of the intensity of the Si peak to that of the E_{2g} peak, $I(Si)/I(E_{2g})$, as a function of thickness H. This dependence can be used as a calibration curve for Raman-based nano-metrology of these films. The approach can be extended to other layered van der Waals materials. For practical purposes, the Raman metrology of exfoliated films is easier and faster than AFM inspection.

Exfoliated thin films of van der Waals materials, other than graphene and boron nitride, have low thermal conductivity. The FQL films of Bi_2Te_3 or MX_2 are not exactly 2D systems like graphene. The phonon transport in such films is normally limited by the extrinsic phonon–boundary scattering from the top and bottom surfaces. As a result, the initially low bulk values of thermal conductivity for Bi_2Te_3 or MX_2

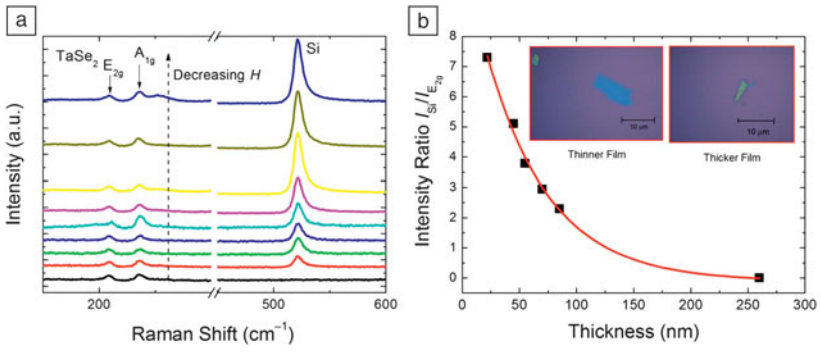


Figure 4. Phonons in thin films of van der Waals materials. (a) Raman spectra of the exfoliated thin films of $TaSe_2$ on a Si substrate. Data are shown for film thicknesses ranging from ~260 nm to below 30 nm. The characteristic E_{2g} and A_{1g} peaks of $TaSe_2$ are clearly observed. The intensity of the Si peak at 522 cm^{-1} increases with decreasing thickness of the $TaSe_2$ film. (b) The ratio of the intensity of the Si peak to that of the E_{2g} peak in the Raman spectrum of $TaSe_2$. The calibrated intensity ratio is used for nano-metrology of $TaSe_2$ films. The insets show optical microscopy images of two flakes of $TaSe_2$ with substantially different thicknesses. The thinner flakes appear blue in color, whereas the thicker flakes appear yellowish.[68]

https://doi.org/10.1557/mrs.2014.169 Published online by Cambridge University Press

decrease further in the exfoliated films. For example, it was found that the RT thermal conductivity of exfoliated $TaSe_2$ films decreases from its bulk value of about 16 W mK^{-1} to ~9 W mK^{-1} in 45-nm-thick films.[68]

Charge density waves in MX_2 thin films

The appearance of the CDW collective electron–phonon state results from a Peierls instability.[66] Below T_P, the atomic lattice undergoes a periodic distortion, and the electrons condense into a collective electron–phonon ground state with a periodic modulation of the charge density leading to an energy gap at the Fermi surface. For small applied electric fields, the CDW remains pinned to defects of the underlying lattice. Above a threshold field, CDW can 'de-pin' from the defects and slide through the crystal, producing a collective current. Materials with CDW effects have been considered for possible use in electronic and optoelectronic devices.[69,70] Interest in CDW microscopic quantum collective states for information processing has recently been renewed.[67,71]

The phonon spectrum undergoes modification below the transition temperature to the CDW regime. The latter is explained by the formation of a "superlattice" with the CDW periodicity. **Figure 5**a presents Raman spectra of the exfoliated $TiSe_2$ film.[67] The main features are the A_{1g} peak at ~207 cm^{-1} and the E_g peak at 233 cm^{-1}. The feature at 316 cm^{-1} is more pronounced and appears as a distinguished peak near the transition temperature. One can also notice that the temperature at which the spectrum modification is observed is shifted to about ~225 K from the bulk value of 190 K. Recording the temperature at which new features in the Raman spectrum appear can provide information on the CDW transition temperature in the exfoliated $TiSe_2$ films. Figure 5b shows that the transition temperature increases from ~200 K in thick films to ~240 K in films with thicknesses below ~100 nm. From the applications point of view, the possibility of increasing T_P in thin films of CDW materials presents a major benefit.

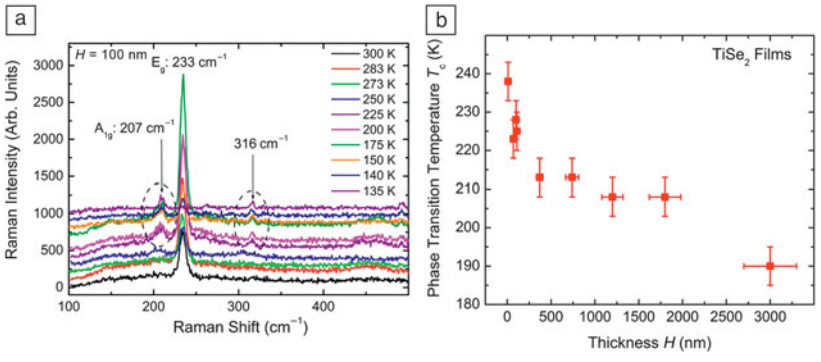


Figure 5. Charge-density wave effects in thin films of transition-metal dichalcogenides. (a) Temperature dependence of the $TiSe_2$ Raman spectrum of a thinner film (thickness, H = 100 nm) in the cooling cycle from 300 K to 135 K. Note the appearance of well-resolved peaks at ~207 cm^{-1} and ~316 cm^{-1} after the temperature decreases below the transition temperature T_C for a given film thickness. The evolution of the Raman spectrum can be used to investigate the dependence of the transition temperature on the thickness of the films. (b) Dependence of the transition temperature to the charge-density wave regime on the $TiSe_2$ film thickness.[67]

Engineering phonons by twisting atomic planes

The excellent heat conduction properties of graphene are finding practical applications in thermal management.[35,72–77] Some of the most promising applications are as fillers in thermal interface materials and heat spreading coatings.[72–77] The phonon thermal transport in graphene and few-layer graphene (FLG) can be strongly affected by defects, isotopes, strain, and geometry of the samples.[35] Another interesting possibility for phonon engineering in FLG and van der Waals materials originates from phonon spectrum modification via twisting atomic planes with respect to each other. Twisting atomic planes change not only acoustic but also optical phonon spectra with corresponding consequences for specific heat, thermal transport, and electron–phonon interactions.[78]

It was theoretically demonstrated that low-energy electron dispersion in twisted bilayer graphene (T-BLG) is linear as in single-layer graphene (SLG) but with reduced Fermi velocity, especially for small rotation angles.[79] The effect of plane twisting on phonons is different. Twisting bilayer graphene leads to emergence of new phonon branches—termed hybrid folded phonons—which originate from the mixing of phonon modes from different high-symmetry directions in the BZ. The frequencies of the hybrid folded phonons depend strongly on the rotation angle and can be used for non-contact identification of the twist angles in graphene samples.[78] The phonon dispersions in AA-stacked BLG and T-BLG with rotation angles $\theta = 21.8°$ are shown in **Figure 6**. In AA-stacked BLG, the carbon atoms of one atomic plane appear exactly above the atoms in another atomic plane.

The unit cell of SLG consists of two atoms, therefore there are six phonon branches in SLG: the out-of-plane transverse acoustic (ZA), out-of-plane transverse optic (ZO), in-plane LA, in-plane TA, in-plane LO, and in-plane TO. In BLG, there are four atoms in the unit cell, and the number of phonon branches is doubled (see Figure 6a). The phonon polarizations of these pairs of branches are denoted as LA_1/LA_2, TA_1/TA_2, ZA_1/ZA_2, LO_1/LO_2, TO_1/TO_2, and ZO_1/ZO_2. These modes, in general, can be understood as the "bilayer" analogs of LA, TA, ZA, LO, TO, and ZO polarizations of SLG, respectively. The energy difference Δ between the phonon branches in the pairs is small due to the weak van der Waals coupling. The number of atoms in the unit cell of T-BLG with $\theta = 21.8°$ increases by a factor of 7 as compared with BLG. The number of phonon branches increases to 84 for T-BLG with $\theta = 21.8°$. The frequencies of the phonon modes depend strongly on the rotational angle, and

https://doi.org/10.1557/mrs.2014.169 Published online by Cambridge University Press

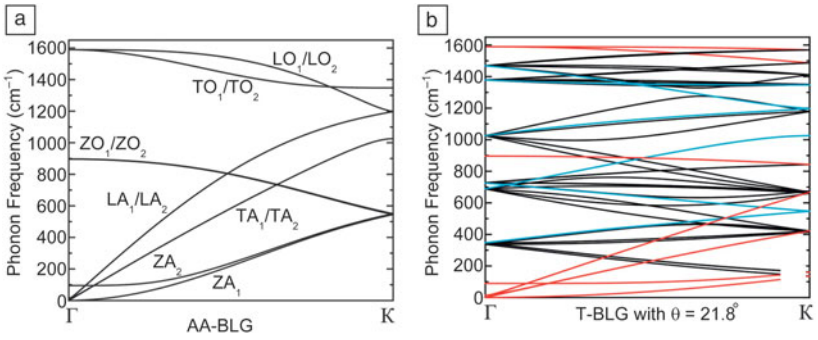


Figure 6. (a) Phonon energy dispersions in AA-stacked bilayer graphene (AA-BLG) and in (b) twisted bilayer graphene (T-BLG) with θ = 21.8°. All dispersion relations are shown for the Γ–*K* direction in the Brillouin zone of BLG and T-BLG. The dispersion was calculated using the Born-von-Karman model for the intralayer atomic interactions and the Lennard-Jones potential for the interlayer interactions. The changes in the phonon dispersion affect the specific heat and thermal conductivity.[78]

their number increases with decreasing angle. It is clear that such drastic modification of the phonon spectrum in T-BLG, even with small variation in the phonon DOS, can result in significant changes in the electron–phonon interactions and phonon transport. This sensitivity to the twist angle opens up new opportunities for phonon engineering of the material properties. The modification of the phonon spectrum in T-BLG has been confirmed experimentally.[80–85]

Summary and outlook

This article presents phonon properties in low-dimensional materials focusing on graphene and van der Waals materials. Possibilities of controlled modification of the phonon dispersion and transport for achieving improved thermal and electronic properties—referred to as phonon engineering—have been discussed. It was argued that quasi 2D materials such as graphene, few-layer graphene (FLG), and metal dichalcogenide thin films offer additional opportunities for phonon engineering as compared to conventional nanostructures. There are numerous indications that the graphene thermal field is already moving to the stage of practical applications. Graphene and FLG flakes produced by an inexpensive liquid-phase exfoliation technique are being utilized as fillers in thermal interface materials and thermal phase-change materials. FLG heat spreaders have been shown to lower the temperature of high-power density field-effect transistors. Hybrid graphene-copper interconnects are capable of performing the dual function of transmitting electrical signals and dissipating the heat generated in the interconnect hierarchy. The optothermal Raman technique developed for thermal conductivity studies of graphene has been extended to a range of van der Waals materials—both suspended and supported on a substrate. It is expected that this technique will add significantly to the knowledge of phonon transport in 2D materials. Micro-Raman spectroscopy, which served exceptionally well as a metrology tool for graphene and FLG, is rapidly becoming an essential characterization tool for 2D materials beyond graphene.

The growing availability of 2D materials and heterostructures made of 2D van der Waals materials creates opportunities for engineering phonon properties at RT. One can expect that controlling phonon transport in such heterostructures will eventually bring practical benefits similar to those achieved by controlling electron transport in modern electronic and optoelectronic devices based on semiconductor quantum confined structures.

Acknowledgments

The work at UC Riverside was supported, in part, by the National Science Foundation (NSF) project ECCS-1307671 on engineering thermal properties of graphene, by DARPA Defense Microelectronics Activity (DMEA) under agreement number H94003–10–2-1003, and by the STARnet Center for Function Accelerated Nano-Material Engineering (FAME)—Semiconductor Research Corporation (SRC) program sponsored by MARCO and DARPA. The work at UC Riverside was supported, in part, by the National Science Foundation (NSF) project ECCS-1307671 on engineering thermal properties of graphene, by DARPA Defense Microelectronics Activity (DMEA) under agreement number H94003–10–2-1003, and by STARnet Center for Function Accelerated NanoMaterial Engineering (FAME)—Semiconductor Research Corporation (SRC) program sponsored by MARCO and DARPA, NSF and SRC Nanoelectronic Research initiative (NRI) project (NSF-1124733): Charge-Density-Wave Computational Fabric: New State Variables and Alternative Material Implementation as a part of the Nanoelectronics for 2020 and beyond (NEB-2020) program, and by UC Proof of Concept project on Graphene-Based Thermal Interface Materials and Heat Spreaders.

References

1. J.M. Ziman, *Electrons and Phonons: The Theory of Transport Phenomena in Solids* (Oxford University Press, New York, 2001).
2. P.G. Klemens, *Solid State Phys.* **7**, 1 (1958).
3. A. Balandin, K.L. Wang, *J. Appl. Phys.* **84**, 6149 (1998).
4. A. Balandin, K.L. Wang, *Phys. Rev. B: Condens. Matter* **58**, 1544 (1998).
5. A.A. Balandin, *J. Nanosci. Nanotechnol.* **5**, 1015 (2005).
6. A.A. Balandin, E.P. Pokatilov, D.L. Nika, *J. Nanoelectron. Optoelectron.* **2**, 140 (2007).
7. T. Klitsner, R.O. Pohl, *Phys. Rev. B: Condens. Matter* **36**, 6551 (1987).
8. E.P. Pokatilov, D.L. Nika, A.A. Balandin, *Appl. Phys. Lett.* **85**, 825 (2004).
9. E.P. Pokatilov, D.L. Nika, A.A. Balandin, *Phys. Rev. B: Condens. Matter* **72**, 113311 (2005).
10. E.P. Pokatilov, D.L. Nika, A.A. Balandin, *Superlattices Microstruct.* **38**, 168 (2005).
11. E.P. Pokatilov, D.L. Nika, A.A. Balandin, *Superlattices Microstruct.* **33**, 155 (2003).
12. H. Benisty, C.M. Sotomayor-Torres, C. Weisbuch, *Phys. Rev. B: Condens. Matter* **44**, 10945 (1991).
13. S.N. Klimin, E.P. Pokatilov, V.M. Fomin, *Phys. Status Solidi B* **190**, 441 (1995).
14. E.P. Pokatilov, D.L. Nika, V.M. Fomin, J.T. Devereese, *Phys. Rev. B: Condens. Matter* **77**, 125328 (2008).
15. S.M. Rytov, Zh. Akust, *Sov. Phys. Acoust.* **2**, 67 (1956).
16. C. Colvard, T.A. Gant, M.V. Klein, R. Merlin, R. Fischer, H. Morkoc, A.C. Gossard, *Phys. Rev. B: Condens. Matter* **31**, 2080 (1985).

https://doi.org/10.1557/mrs.2014.169 Published online by Cambridge University Press

17. N. Bannov, V. Mitin, M. Stroscio, *Phys. Status Solidi B* **183**, 131 (1994).
18. N. Nishiguchi, Y. Ando, M.N. Wybourne, *J. Phys. Condens. Matter* **9**, 5751 (1997).
19. A. Svizhenko, A. Balandin, S. Bandyopadhyay, M.A. Stroscio, *Phys. Rev. B: Condens. Matter* **57**, 4687 (1998).
20. J.V.D. Veliadis, J.B. Khurgin, Y.J. Ding, *IEEE J. Quantum Electron.* **32**, 1155 (1996).
21. J. Zou, A. Balandin, *J. Appl. Phys.* **89**, 2932 (2001).
22. A.A. Balandin, *Phys. Low Dimen. Struct.* **5**/6, 73 (2000).
23. V.A. Fonoberov, A.A. Balandin, *Nano Lett.* **6**, 2442 (2006).
24. D.L. Nika, E.P. Pokatilov, A.A. Balandin, *Appl. Phys. Lett.* **93**, 173111 (2008).
25. N.D. Zincenco, D.L. Nika, E.P. Pokatilov, A.A. Balandin, *J. Phys. Conf. Ser.* **92**, 012086 (2007).
26. D.L. Nika, N.D. Zincenko, E.P. Pokatilov, *J. Nanoelectron. Optoelectron.* **4**, 180 (2009).
27. O.L. Lazarenkova, A.A. Balandin, *Phys. Rev. B: Condens. Matter* **66**, 245319 (2002).
28. A.A. Balandin, O.L. Lazarenkova, *Appl. Phys. Lett.* **82**, 415 (2003).
29. D.L. Nika, E.P. Pokatilov, *Phys. Rev. B: Condens. Matter* **84**, 165415 (2011).
30. E.P. Pokatilov, D.L. Nika, A.A. Balandin, *Appl. Phys. Lett.* **89**, 113508 (2006).
31. E.P. Pokatilov, D.L. Nika, A.A. Balandin, *Appl. Phys. Lett.* **89**, 112110 (2006).
32. M. Hu, K.P. Giapis, J.V. Goicochea, X. Zhang, D. Poulikakos, *Nano Lett.* **11**, 618 (2011).
33. M.C. Wingert, Z.C.Y. Chen, E. Dechaumphai, J. Moon, J.-H. Kim, J. Xiang, R. Chen, *Nano Lett.* **11**, 5507 (2011).
34. A.A. Balandin, S. Ghosh, W. Bao, I. Calizo, D. Teweldebrhan, F. Miao, C.N. Lau, *Nano Lett.* **8**, 902 (2008).
35. A.A. Balandin, *Nat. Mater.* **10**, 569 (2011).
36. S. Ghosh, I. Calizo, D. Teweldebrhan, E.P. Pokatilov, D.L. Nika, A.A. Balandin, W. Bao, F. Miao, C.N. Lau, *Appl. Phys. Lett.* **92**, 151911 (2008).
37. D.L. Nika, E.P. Pokatilov, A.S. Askerov, A.A. Balandin, *Phys. Rev. B: Condens. Matter* **79**, 155413 (2009).
38. D.L. Nika, S. Ghosh, E.P. Pokatilov, A.A. Balandin, *Appl. Phys. Lett.* **94**, 203103 (2009).
39. L. Lindsay, D.A. Broido, N. Mingo, *Phys. Rev. B: Condens. Matter* **82**, 115427 (2010).
40. P.G. Klemens, *J. Wide Bandgap Mater.* **7**, 332 (2000).
41. P.G. Klemens, *Int. J. Thermophys.* **22**, 265 (2001).
42. S. Ghosh, W. Bao, D.L. Nika, S. Subrina, E.P. Pokatilov, C.N. Lau, A.A. Balandin, *Nat. Mater.* **9**, 555 (2010).
43. D.L. Nika, A.S. Askerov, A.A. Balandin, *Nano Lett.* **12**, 3238 (2012).
44. D.L. Nika, A.A. Balandin, *J. Phys. Condens. Matter* **24**, 233203 (2012).
45. S. Berber, Y.-K. Kwon, D. Tománek, *Phys. Rev. Lett.* **84**, 4613 (2000).
46. W. Cai, A.L. Moore, Y. Zhu, X. Li, S. Chen, L. Shi, R.S. Ruoff, *Nano Lett.* **10**, 1645 (2010).
47. L.A. Jaureguia, Y. Yueb, A.N. Sidorovc, J. Hud, Q. Yue, G. Lopezf, R. Jalilianf, D.K. Benjaming, D.A. Delkdg, W. Wuh, Z. Liuh, X. Wangi, Z. Jiangj, X. Ruank, J. Baol, S.S. Peil, Y.P. Chenm, *ECS Trans.* **28**, 73 (2010).
48. S. Chen, Q. Wu, C. Mishra, J. Kang, H. Zhang, K. Cho, W. Cai, A.A. Balandin, R.S. Ruoff, *Nat. Mater.* **11**, 203 (2012).
49. J.H. Seol, I. Jo, A.L. Moore, L. Lindsay, Z.H. Aitken, M.T. Pettes, X. Li, Z. Yao, R. Huang, D. Broido, N. Mingo, R.S. Ruoff, L. Shi, *Science* **328**, 213 (2010).
50. P. Blake, E.W. Hill, A.H. Castro Neto, K.S. Novoselov, D. Jiang, R. Yang, T.J. Booth, A.K. Geim, *Appl. Phys. Lett.* **91**, 063124 (2007).
51. X. Li, C.W. Magnuson, A. Venugopal, R.M. Tromp, J.B. Hannon, E.M. Vogel, L. Colombo, R.S. Ruoff, *J. Am. Chem. Soc.* **133**, 2816 (2011).
52. X. Li, W. Cai, L. Colombo, R.S. Ruoff, *Nano Lett.* **9**, 4268 (2009).
53. K.S. Novoselov, D. Jiang, F. Schedin, T.J. Booth, V.V. Khotkevich, S.V. Morozov, A.K. Geim, *Proc. Natl. Acad. Sci. U.S.A.* **102**, 10451 (2005).
54. K.S. Novoselov, E. McCann, S.V. Morozov, V.I. Fal'ko, M.I. Katsnelson, U. Zeitler, D. Jiang, F. Schedin, A.K. Geim, *Nat. Phys.* **2**, 177 (2006).
55. A.K. Geim, I.V. Grigorieva, *Nature* **499**, 419 (2013).
56. D. Teweldebrhan, V. Goyal, A.A. Balandin, *Nano Lett.* **10**, 1209 (2010).
57. R. Mas-Balleste, C. Gomez-Navarro, J. Gomez-Herrero, F. Zamora, *Nanoscale* **3**, 20 (2011).
58. K.J. Koski, Y. Cui, *ACS Nano* **7**, 3739 (2013).
59. M. Xu, T. Liang, M. Shi, H. Chen, *Chem. Rev.* **113**, 3766 (2013).
60. D. Teweldebrhan, V. Goyal, M. Rahman, A.A. Balandin, *Appl. Phys. Lett.* **96**, 053107 (2010).
61. K.M.F. Shahil, M.Z. Hossain, D. Teweldebrhan, A.A. Balandin, *Appl. Phys. Lett.* **96**, 153103 (2010).
62. V. Goyal, D. Teweldebrhan, A.A. Balandin, *Appl. Phys. Lett.* **97**, 133117 (2010).
63. W. Richter, H. Kohler, C.R. Becker, *Phys. Status Solidi B* **84**, 619 (1977).
64. V. Wagner, G. Dolling, B.M. Powell, G. Landwehr, *Phys. Status Solidi B* **85**, 311 (1978).
65. M. Chhowalla, H.S. Shin, G. Eda, L.-J. Li, K.P. Loh, H. Zhang, *Nat. Chem.* **5**, 263 (2013).
66. G. Gruner, *Rev. Mod. Phys.* **60**, 1129 (1988).
67. P. Goli, J. Khan, D. Wickramaratne, R.K. Lake, A.A. Balandin, *Nano Lett.* **12**, 5941 (2012).
68. Z. Yang, C. Jiang, T. Pope, C. Tsang, J.L. Stickney, P. Goli, J. Renteria, T. Salguero, A.A. Balandin, *J. Appl. Phys.* **114**, 204301 (2013).
69. D. Mihailovic, D. Dvorsek, V.V. Kabanov, J. Demsar, L. Forro, H. Berger, *Appl. Phys. Lett.* **80**, 871 (2002).
70. N. Ogawa, K. Miyano, *Appl. Phys. Lett.* **80**, 3225 (2002).
71. J. Renteria, R. Samnakay, C. Jiang, T.R. Pope, P. Goli, Z. Yan, D. Wickramaratne, T.T. Salguero, A.G. Khitun, R.K. Lake, A.A. Balandin, *J. Appl. Phys.* **115**, 034305 (2014).
72. K.M.F. Shahil, A.A. Balandin, *Nano Lett.* **12**, 861 (2012).
73. V. Goyal, A.A. Balandin, *Appl. Phys. Lett.* **100**, 073113 (2012).
74. Z. Yan, G. Liu, J.M. Khan, A.A. Balandin, *Nat. Commun.* **3**, 827 (2012).
75. K.M.F. Shahil, A.A. Balandin, *Solid State Commun.* **152**, 1331 (2012).
76. P. Goli, S. Legedza, A. Dhar, R. Salgado, J. Renteria, A.A. Balandin, *J. Power Sources* **248**, 37 (2014).
77. P. Goli, H. Ning, X. Li, C.Y. Lu, K.S. Novoselov, A.A. Balandin, *Nano Lett.* **1**, 1 (2014).
78. A.I. Cocemasov, D.L. Nika, A.A. Balandin, *Phys. Rev. B: Condens. Matter* **88**, 035428 (2013).
79. J.M.B. Lopes dos Santos, N.M.R. Peres, A.H. Castro Neto, *Phys. Rev. Lett.* **99**, 256802 (2007).
80. A.K. Gupta, Y. Tang, V.H. Crespi, P.C. Eklund, *Phys. Rev. B: Condens. Matter* **82**, 241406 (R) (2010).
81. A. Righi, S.D. Costa, H. Chacham, C. Fantini, P. Venezuela, C. Magnuson, L. Colombo, W.S. Basca, R.S. Ruoff, M.A. Pimenta, *Phys. Rev. B: Condens. Matter* **84**, 241409 (R) (2011).
82. V. Carozo, C.M. Almeida, E.H.M. Ferreira, L.G. Cancado, C.A. Achete, A. Jorio, *Nano Lett.* **11**, 4527 (2011).
83. C.-C. Lu, Y.-C. Lin, Z. Liu, C.-H. Yeh, K. Suenaga, P.-W. Chiu, *ACS Nano* **7**, 2587 (2013).
84. J. Campos-Delgado, L.C. Cancado, C.A. Achete, A. Jorio, J.-P. Raskin, *Nano Res.* **6**, 269 (2013).
85. Y. Wang, Z. Su, W. Wu, S. Nie, N. Xie, H. Gong, Y. Guo, J.H. Lee, S. Xing, X. Lu, H. Wang, X. Lu, K. McCarty, S.-S. Pei, F. Robles-Hernandez, V.G. Hadjiev, J. Bao, *Appl. Phys. Lett.* **103**, 123101 (2013). □



Alexander A. Balandin is the University of California Presidential Chair Professor of Electrical Engineering and Founding Chair of Materials Science and Engineering at the University of California–Riverside. He received his MS degree (1991) in applied physics and mathematics from the Moscow Institute of Physics and Technology and his PhD degree (1997) in electrical engineering from the University of Notre Dame. His research interests are in the area of advanced materials, nanostructures, and devices for electronic, optoelectronic, and energy applications. He is the recipient of the MRS Medal (2013), IEEE Pioneer Award in Nanotechnology (2011), as well as the NSF CAREER Award, ONR Young Investigator Award, and Merrill Lynch Innovation Award. He is a Fellow of APS, MRS, IEEE, SPIE, OSA, IOP, and AAAS. He is an editor of *IEEE Transactions on Nanotechnology* and an associate editor of *Applied Physics Letters.* Balandin can be reached at the Department of Electrical Engineering and Materials Science and Engineering Program, Bourns College of Engineering, University of California–Riverside, USA; tel. 951-827-2351; and email balandin@ee.ucr.edu.

GET SOCIAL www.mrs.org/social-media

https://doi.org/10.1557/mrs.2014.169 Published online by Cambridge University Press